Bioavailability of molybdenite to support nitrogen fixation on early Earth by an anoxygenic phototroph

Xinyi Zhou[1], Yizhi Sheng[1,2]*, Yanning Zheng[3], Mingyue Jiang[3], Mengmei Wang[3,4], Zihua Zhu[5], Gaoyuan Li[1], Oliver Baars[6], and Hailiang Dong[1,2]*

[1] Center for Geomicrobiology and Biogeochemistry Research, State Key Laboratory of Biogeology and Environmental Geology, China University of Geosciences, Beijing 100083, China.

[2] Frontiers Science Center for Deep-time Digital Earth, China University of Geosciences, Beijing 100083, China

[3] State Key Laboratory of Microbial Resources, Institute of Microbiology, Chinese Academy of Sciences, Beijing 100101, China.

[4] College of Life Sciences, University of Chinese Academy of Sciences, Beijing 100049, China.

[5] Pacific Northwest National Laboratory, Richland, Washington 99352, United States.

[6] Department of Entomology and Plant Pathology, North Carolina State University, Raleigh, North Carolina, 27695, United States.

***Corresponding Authors:** Yizhi Sheng & Hailiang Dong

Email: shengyz@cugb.edu.cn & dongh@cugb.edu.cn

ABSTRACT

Biological nitrogen fixation, which converts atmospheric dinitrogen to ammonia, is catalyzed mostly by Mo-nitrogenase and is a primary contributor to bioavailable nitrogen on early Earth. Mo-nitrogenase is believed to have evolved during the Archean, despite the extremely low concentration of dissolved Mo. However, it remains unclear whether Mo minerals could serve as a source of Mo to support the prevalence of Mo-nitrogenase on early Earth. Here we investigated the bioavailability of molybdenite by incubating it with a metabolically ancient anoxygenic phototroph (*Rhodopseudomonas palustris*) under anoxic conditions. In the laboratory, *R. palustris* utilized molybdenum from molybdenite as a cofactor for nitrogen fixation. This bacterium extracted Mo from molybdenite by secreting molybdophores rhodopetrobactin A and B and by expressing Mo transport proteins. Surface-sensitive techniques demonstrated significant changes in surface chemistry of molybdenite after its interaction with cells. These findings provide novel explanations for the prevalence of Mo-nitrogenase on early Earth, with significant implications for nitrogen fixation in modern Mo-deficient environments.

Keywords: Archean ocean, Mo bioavailability, molybdenite, nitrogen fixation, *Rhodopseudomonas palustris*

1. Introduction

Bioavailable nitrogen was believed to be one of limiting nutrients on early Earth (Canfield et al. 2010). Abiotic nitrogen fixation, mainly via lightning, meteor impacts, photocatalysis by Fe-S minerals, or hydrothermal reduction (Stüeken et al. 2016), was considered insufficient to meet the increasing nitrogen requirement of the early biosphere (Canfield et al. 2010; Yang et al. 2019). Biological nitrogen fixation, performed by a group of specialized prokaryotes known as diazotrophs (Boyd et al. 2011), was an essential process to supply bioavailable nitrogen to the expanding biosphere (Rucker and Kacar 2023). This process is catalyzed by a metalloenzyme called nitrogenase, which is categorized into three forms based on the metal cofactor in its active site: Mo-nitrogenase, V-nitrogenase, and Fe-nitrogenase. Most nitrogenases use Mo as their metal cofactor due to its highest energetic efficiency (Demtroder et al. 2019). Therefore, Mo availability is essential to global biological nitrogen fixation (Barron et al. 2008; Ward 2012).

Before the Great Oxidation Event (GOE) approximately 2.3-2.5 billion years ago, dissolved Mo was scarce in Archean ocean (< 2-3 nM) (Anbar 2008; Johnson et al. 2021), mostly from submarine hydrothermal vents (Evans et al. 2023; Huston et al. 2001) and limited weathering of sulfidic minerals (Helz et al. 2011; Johnson et al. 2021). At this Mo level, biological nitrogen fixation is significantly inhibited (Nishizawa et al. 2014; Sheng et al. 2023; Zerkle et al. 2006; Glass et al., 2012). After the GOE, oxidative weathering increased dissolved Mo levels, making it one of the most abundant trace metals in modern oceans (~100 nM) (Anbar 2008). Therefore, it was traditionally believed that Mo-nitrogenase evolved after the GOE, later than the Fe-nitrogenase because of abundant aqueous Fe in Archean ocean (Canfield et al. 2010; Garcia et al. 2020). However, nitrogen isotope ratios in Archean sediments suggested that Mo-nitrogenase originated nearly 3.2 billion years ago (Stueken et al. 2015). Interestingly, phylogenetic analysis of all nitrogenases independently confirmed that Mo-nitrogenase was the earliest evolved nitrogenase (Boyd et al. 2011; Garcia et al. 2020), dating back to the Mesoarchean (Parsons et al. 2021). All these studies suggest that Mo-nitrogenase emerged in an aqueous Mo-depleted environment (Mus et al. 2019). Therefore, a possible scenario to reconcile this apparent paradox is that early microorganisms may be able to acquire Mo from minerals and rocks.

Indeed, throughout the long geological history, microorganisms have developed strategies to obtain nutrients from minerals and rocks to support their growth and metabolism (Dong et al. 2022; Uroz et al. 2009). Strategies of metal acquisition from solids include redox reactions, acidification, and/or secretion of metal-chelating ligands such as metallophores (Dong et al. 2022). For instance, to compensate for the iron (Fe) scarcity in oxic and neutral pH conditions, certain microorganisms can secrete siderophores to obtain Fe from minerals (Kraemer et al. 2014; Manck et al. 2022). Metal acquisition by these high-

affinity ligands extends to other metals such as Cu [i.e., methanobactin (Mb)] (Knapp et al. 2007) and Mo (Kraemer et al. 2014).

An aerobic diazotroph, *Azotobacter vinelandii*, uses Mo from Mo-rich synthetic silicate glass and molybdenite (MoS_2) for nitrogen fixation, likely through secretion of siderophores (also termed molybdophore) that are capable of binding both Fe and Mo (Liermann et al. 2005; Srivastava et al. 2023). However, under oxic conditions, molybdenite can be partially oxidized to form more soluble Mo oxides (Rickard 2012). In contrast, under anoxic conditions, molybdenite is believed to be insoluble (Greber et al. 2015), rendering it unavailable to support diazotrophic growth. At present, only one anaerobic diazotroph *Clostridium kluyveri* has been identified that can utilize Mo from molybdenite for nitrogen fixation, with the help of metal-chelating metabolites while the specific types of these metabolites remain unknown (Sheng et al. 2023).

Before the evolution of oxygenic photosynthesis (Sánchez-Baracaldo and Cardona 2019), anoxygenic phototrophic bacteria may have been the primary nitrogen fixers on early Earth (Cardona 2019; Planavsky et al. 2021), suggesting that they could fix nitrogen under Mo-depleted conditions. In an analog environment of Proterozoic ocean with low Mo (<10 nM), nitrogen fixation was exclusively catalyzed by anoxygenic phototrophs using Mo-nitrogenase (Philippi et al. 2021). Therefore, these organisms may have developed strategies to use other sources of Mo, yet the processes and underlying mechanisms remain unknown. Among anoxygenic phototrophs, *Rhodopseudomonas palustris* is known to produce metallophores under metal-depleted conditions (Baars et al. 2018).

The overarching goal of this study was therefore to test whether Mo-bearing minerals could serve as a source of Mo for nitrogen fixation by an anoxygenic phototroph. Our experimental approach was to incubate a model bacterium *R. palustris* with molybdenite under diazotrophic conditions. The N_2 fixation rate was measured by acetylene reduction assay (ARA) and ^{15}N labeled methods. Trace metal mobilization, cellular uptake, and metallophore production were analyzed, along with proteomics analysis, microscopic imaging, and mineral surface chemistry, to uncover the potential mechanisms of microbial acquisition of Mo from minerals. The results provide important insights into the bioavailability of solid-source Mo to drive the nitrogen cycling on early Earth as well as in modern Mo-deficient environments.

2. Materials and methods

2.1 Bacterial strain and growth medium

R. palustris is one of a few bacteria that have all three nitrogenases (Mo-, V-, and Fe-) (Larimer et al. 2004; Oda et al. 2005). Metal availability usually dictates the type of

111 nitrogenase expressed in this bacterium (Oda et al. 2005). Because Mo-nitrogenase contains
112 Fe, i.e., FeMo-co, aqueous Fe is still needed in medium when solid-source Mo is supplied as
113 the only source of Mo (Sheng et al. 2023; Srivastava et al. 2023). However, this creates an
114 ambiguity, if solid source Mo is not bioavailable, the organism may switch to Fe-nitrogenase
115 (FeFe-co) and still performs nitrogen fixation (Oda et al. 2005). To eliminate this ambiguity, a
116 mutant was created, where the Fe-nitrogenase gene (*anfA*) in wildtype *R. palustris* CGA009
117 was knocked out to obtain *R.palustris* CGA009-Δ*anfA.* This mutant expresses Mo-nitrogenase
118 and V-nitrogenase, but not Fe-nitrogenase (Table S1). To check whether the background V
119 supported V-nitrogenase expression, *R. palustris* CGA766 (only express V-nitrogenase) was
120 constructed. The details for CGA009-ΔanfA mutant and CGA766 mutant construction can be
121 found in Supporting Information (SI) Section S1.

122 Prior to experiments, glassware was soaked in HNO_3 (5% v/v) for 24 hours and washed
123 with deionized H_2O to remove any potential metal contamination. A normal medium used to
124 grow cell cultures was modified from a previous study (Oda et al. 2005) by removing EDTA
125 and NTA in SI Section S2.

126 To evaluate the effect of molybdenite on nitrogen fixation, it is essential to minimize Mo
127 levels from all chemicals used to make the growth medium. To achieve this, 8-
128 hydroxyquintoline (8-HQ) was used as a Mo scavenging reagent (SI Section S2). The resulting
129 Mo-depleted medium [2 nM, as determined by inductively coupled plasma mass
130 spectrometry (ICP-MS, PerkinElmre Nex10N 300X)] was used for subsequent nitrogen-
131 fixation experiments. Vanadium (V) remained undetected (<0.5 nM).

132 *R. palustris* CGA009-Δ*anfA* strain was initially grown under anoxic and light conditions in
133 the normal growth medium at 30 °C to yield the maximum growth (Oda et al. 2005). Details
134 for growth medium was included in SI Section S2. Afterwards, nitrogen-fixing (diazotrophic)
135 mode was established using the same medium but with aqueous and solid-source Mo
136 instead of $(NH_4)_2SO_4$.

137

138 *2.2 Preparation of mineral*

139 Molybdenite (MoS_2), which was the primary Mo mineral on early Earth (maximum age
140 4.568 Ga) (Hazen et al. 2014), was used as a model mineral. Molybdenite was size-
141 fractionated to obtain 0.075-0.16 mm size fraction. Nanoparticles smaller than 2 µm were
142 removed via centrifugation (4,000 g for 7 mins). This size fraction was washed three times
143 with deionized water and once with fresh metal-depleted medium to remove any
144 molybdenum oxides possibly present on the surface. Minerals were then autoclaved and
145 preserved in a COY anoxic chamber (98% N_2 and 2% H_2, Coy Laboratory Products, Grass Lake,
146 Michigan).

147

148 *2.3 Experimental setup*

149 Normally grown *R. palustris* CGA009-Δ*anfA* was initially transferred to Mo-depleted
150 medium for at least 3 times to exhaust any residual cell-associated Mo and Fe. After the last
151 transfer, 0.4 mL cell culture (by volume) was inoculated into 20 mL medium in 50-mL anoxic
152 vials containing two forms of Mo (Na_2MoO_4 and mineral) and 2.5 µM $FeSO_4 \cdot 7H_2O$.

153 To evaluate the effect of aqueous Mo on growth of *R. palustris* CGA009-Δ*anfA*, a Mo
154 concentration gradient, ranging from 2 nM (measured in Mo-depleted medium) to 10 µM,
155 was used. This range brackets those in natural environments: ~2 nM in Archean ocean, 0.01
156 µM in euxinic conditions, 0.1 µM in the modern open ocean, 1 µM in geothermal
157 groundwater, and 10 µM in mining/mineralized aquifers (Smedley and Kinniburgh 2017).

158 To ascertain the bioavailability of Mo in minerals, aqueous Mo was replaced with
159 molybdenite at two concentrations: 16 mg/L and 160 mg/L. These two concentrations were
160 chosen because preliminary experiments revealed abiotic molybdenite dissolution at time
161 zero to generate an aqueous Mo concentration of 0.01 µM (typical in euxinic environments)
162 and 0.1 µM (typical in the open ocean), respectively. The normal diazotrophic medium with
163 0.1 µM aqueous Mo served as a positive control, and the negative control did not contain
164 any additional aqueous Mo (but with background Mo of 2 nM).

165 To delineate whether microorganisms facilitated molybdenite dissolution by secreting
166 soluble metabolites, a separate experiment was conducted by using a supernatant collected
167 from microbial incubation of molybdenite. The supernatant was collected via centrifugation
168 (6,000 g for 10 mins) after the cell culture had reached the stationary phase. Fresh
169 molybdenite was then added to the supernatant and allowed to react for 24 hours.
170 Molybdenite concentration was kept the same as in the mineral experiments. A no-cell
171 medium containing only molybdenite was used as a control.

172

173 *2.4 Determination of cell growth, nitrogenase activity, and trace metal concentrations*

174 Cell growth was monitored by measuring optical density at OD=600 nm. Total protein
175 concentration was measured as an alternative method for monitoring time-course change of
176 biomass (SI Section S3).

177 Nitrogenase activity was measured using the acetylene reduction assay (ARA) and $^{15}N_2$
178 tracer method (Mohr et al. 2010). For the ARA determination, 10 mL cell suspensions were
179 incubated in a 26 mL anoxic glass tube with a headspace containing 2% acetylene and 98%
180 helium as previously described (Sheng et al. 2023). Ethylene concentration was measured by

181 using gas chromatography (GC, Agilent 7890A). N_2 fixation rates were measured using a
182 modified $^{15}N_2$ tracer method (Mohr et al. 2010) (SI Section S4).

183 Extracellular and cell-associated Mo concentrations were determined by using ICP-MS
184 (Perkin Elm Nex10N 300X) (SI Section S5). For abiotic experiments, only dissolved Mo was
185 measured.

186

187 *2.5 Characterization and quantification of metallophores*

188 To measure siderophore concentration as a microbial strategy for metal acquisition from
189 minerals, supernatants were collected from cell-mineral incubation experiments, centrifuged
190 (7,000 g for 10 mins), and extracted using solid phase extraction (SPE) cartridges at neutral
191 pH (7.5) (Sheng et al. 2023). The SPE column was Bond Eult C18 (Agilent), known for its high
192 retention of non-polar compounds. Compounds retained in SPE column were eluted
193 sequentially with a mixture of 2 mL 30% and 4 mL 80% methanol. After freeze drying, the
194 samples were reconstituted in 3% methanol and stored at -20 °C until analysis. Any
195 hydrophilic compounds would flow through the column and separately collected.

196 Total siderophore concentrations were determined by Chrome Azurol S (CAS) assay
197 (Perez-Miranda et al. 2007). Deferoxamine mesylate was used as a standard. Two negative
198 controls were prepared for siderophore measurement: 1) normal growth medium; 2) 3%
199 methanol, matching its concentration in the reconstituted SPE samples. To quantify
200 siderophore concentration, reconstituted extracts were analyzed by using high performance
201 liquid chromatography (HPLC) (SI Section S6). 3,4-dihydroxybenzoic acid (DHBA) was used as
202 a standard for determination of siderophore concentration (Baars et al. 2018).

203 Chemical composition of any other microbial metabolites was analyzed by using
204 Orbitrap liquid chromatography (LC-MS) (SI Section S6). Full-scan mass spectra were
205 acquired in both positive ion and negative ion modes (m/z=200-2000). To determine
206 concentrations of metal-chelating metabolites, liquid chromatography-inductively coupled
207 plasma-mass spectrometry (LC-ICP-MS) was used (Supporting Information Section S6).
208 Protochelin was used as a standard to complex Mo and Fe. Stock solutions were prepared by
209 equimolar additions of Na_2MoO_4 and $FeCl_3$ to protochelin (100 µM).

210

211 *2.6 Proteomic analysis*

212 To compare any differences in protein expression patterns between different forms of
213 Mo, proteomic analysis was conducted. Protein from the end of exponential phase was
214 extracted and purified (SI Section S7). Proteomic analysis was performed using LC-MS/MS
215 with an Orbitrap mass spectrometer (Q-Exactive Plus, Thermo Fisher Scientific) connected to

216 a nano-electrospray ion source (Nanospray Flex, Proxeon Biosystems, Odense, Demark) (SI
217 Section S8). All MS raw data were analyzed using MaxQuant and Perseus software (Cox et al.
218 2011).

219

220 *2.7 Mineral characterization*

221 To investigate mineralogical changes of molybdenite after its incubation with cells, X-ray
222 diffraction (XRD, Rigaku-D/MAX-PC 2500, Japan) was performed with a powder X-ray
223 diffractometer using Cu Ka radiation with power of 1000W (40 kV and 25 mA). Samples were
224 scanned in the 2-theta range from 4 to 40 stepping at 0.01 with a count time of 1 s per step.

225 Scanning electron microscopy (SEM) was utilized to visualize any physical associations
226 between cells and molybdenite using a Zeiss Supra 55 scanning electron microscope (SI
227 Section S9). Elemental mapping was performed using a Zeiss Supra 55 SAPPHIRE SEM with a
228 Gensis 2000 X-ray energy dispersive spectrometer (SEM-EDS).

229 Mineral surface chemistry before and after interaction with cells was characterized by
230 using X-ray photoelectron spectroscopy (XPS) (SI Section S10). To further characterize the
231 molecular information on the mineral surface, Time of flight secondary ion mass
232 spectrometry (TOF-SIMS) was used (SI Section S11). Pure molybdenite was also analyzed for
233 comparison.

234

235 3. Results

236 *3.1 Effects of dissolved Mo on nitrogen fixation*

237 V-nitrogenase-only *R.palustris* CGA766 did not grow in the experimental medium
238 (data not shown), indicating that the background level of V (<0.5 nM) was inadequate to
239 sustain V-based nitrogen fixation. Therefore, when using *R.palustris* CGA009-*ΔanfA*, any
240 detected nitrogen fixation should be solely attributed to activation of Mo-nitrogenase.

241 The diazotrophic growth of *R.palustris* CGA009-*ΔanfA* was dependent on the
242 concentrations of aqueous Mo (Fig. 1a). When neither Mo nor Fe was added, the nitrogen
243 fixation rate, as indicated by ethylene production rate, was minimal. Addition of Fe resulted
244 in a small increase in nitrogen fixation rate, suggesting that there may be some residual Mo
245 (~2 nM) either in the medium or associated with cells. Upon addition of Mo, the nitrogen
246 fixation rate increased, with the extent of increase depending on Mo concentration (Fig.1a).
247 There was a logarithmic correlation between nitrogen fixation rate and Mo concentration
248 (Fig. 1b), suggesting greater Mo concentration resulted in a higher nitrogen fixation rate.

249 Consistently, with cell growth, Mo was consumed, leading to a decrease in its
250 concentration over the course of the experiments (Fig. 1c). A higher concentration of initial
251 aqueous Mo resulted in more cell-associated Mo (Figs. 1d and S1a). There was a
252 stoichiometric mass balance between loss of aqueous Mo and association of Mo with cells
253 (Fig. S1b). These data suggested that Mo was either assimilated into the cells, or adhered to
254 their external surface. At the highest Mo concentration of 10 µM, the cell-associated Mo
255 level reached approximately 36.0 µmol mg protein^{-1} (Fig. 1d). A significant positive
256 correlation was observed between nitrogen fixation rate and cell-associated Mo
257 concentration (Fig. 1b), suggesting that Mo was a key determinant for nitrogen fixation.

258

259 *3.2 Effects of molybdenite on nitrogen fixation*

260 The effect of solid-source Mo on nitrogen fixation was evaluated by replacing dissolved
261 Mo with molybdenite. The growth and nitrogen fixation rate of *R. palustris* CGA009-*ΔanfA*
262 varied with molybdenite concentration (Fig. 2). Growth was negligible in the negative control
263 (-Fe -Mo) but maximal in the positive control (+Fe +Mo, 0.1 µM aqueous Mo) (Fig.2a). At a
264 mineral concentration of 16 mg/L, *R.palustris* cells exhibited a substantial growth, albeit at a
265 slower rate than that in the positive control (Fig. 2a). The fastest growth rate occurred at a
266 mineral concentration of 160 mg/L, even surpassing that of the positive control.

267 Consistent with the cell growth curves, the negative control showed the lowest nitrogen
268 fixation rates of 148.0 nmol h^{-1} mg protein^{-1} (ARA) and 5.5 µmol h^{-1} mg protein^{-1} (^{15}N tracer
269 method) (Fig. 2b). Addition of aqueous Mo and Fe increased the rate by 133.5% and 193.6%,
270 as measured by ARA and ^{15}N tracer method, respectively. With molybdenite as the sole Mo
271 source, nitrogen fixation rate further increased. The highest nitrogen fixation rate was
272 measured at the highest mineral concentration of 160 mg/L, i.e., 746.2 nmol h^{-1} mg protein^{-1}
273 (ARA) and 29.0 µmol h^{-1} mg protein^{-1} (^{15}N tracer) (Fig. 2b). This result suggested that mineral-
274 bound Mo was bioavailable and significantly enhanced the nitrogen fixation rate.

275 Upon interaction with cells, extracellular aqueous Mo concentration displayed time-
276 dependent changes (Fig. 2c). Expectedly, only 2 nM Mo (background concentration) was
277 observed in the negative control. In the positive control (0.1 µM Mo), Mo concentration
278 declined overtime, and was completely consumed by 140 hours. In the presence of 16 mg/L
279 molybdenite, aqueous Mo concentration increased in the first 50 hours (Fig. 2c), which
280 corresponded to little cell growth (Fig. 2a). During this period, the rate of Mo consumption
281 was likely lower than that of Mo dissolution, resulting in a net Mo accumulation. From 48 to
282 96 hours, aqueous Mo concentration declined to below the detection limit (< 0.5 nM) (Fig.
283 2c), likely because the rate of consumption exceeded the rate of dissolution (Fig. 2a). When
284 the molybdenite concentration increased to 160 mg/L, aqueous Mo concentration
285 significantly increased over the entire experimental duration, despite active cell growth,

286 suggesting that the amount of Mo released from molybdenite dissolution exceeded the
287 cellular demand of Mo to result in a net Mo accumulation in solution.

288 Expectedly, cell-associated Mo concentration was highest in the 160 mg/L mineral
289 experiment, followed by the lower mineral concentration group (16 mg/L) and the positive
290 control (Fig. 2d). Similar to the aqueous Mo case, a significant positive correlation was
291 observed between nitrogen fixation rate and cell-associated Mo concentration (Fig. S2).

292

293 *3.3 Metallophore production in response to varying Mo conditions*

294 A pH decline induced by microbially produced organic acids could possibly enhance
295 mineral dissolution (Dong et al. 2022) and nitrogen fixation. However, during the cell-mineral
296 incubation, the pH increased from 6.8 to 8, which was unlikely to dissolve molybdenite. A
297 separate abiotic control experiment confirmed negligible Mo dissolution when pH increased
298 from 6.8 to 8 under anoxic conditions (data not shown), consistent with molybdenite
299 stability within this pH range (Hao et al. 2019). Therefore, cells must have employed other
300 strategies to access Mo from molybdenite to support its nitrogen fixation.

301 *R. palustris* is known to secrete metal-chelating siderophores (Baars et al. 2018), which
302 can dissolve molybdenite. Indeed, a yellow color was observed in the positive and mineral
303 groups (Fig. S3), which was expected when the catechol group of siderophores was chelated
304 with Mo (Doydora et al. 2022). Such color was not observed in the negative control, likely
305 because there was no Mo in this control, not because of lack of siderophores in this group.

306 To determine whether such siderophores facilitated molybdenite dissolution, a separate
307 control experiment was conducted by incubating molybdenite with the supernatants
308 collected from the negative control and mineral groups (positive control was not included).
309 Indeed, significantly more aqueous Mo was measured after incubation of molybdenite with
310 the supernatants from both groups, reaching ~0.55 µM after 24 hours, approximately 40%
311 higher than that in the abiotic control (Fig. 3a).

312 To explore the form of Mo-siderophore complexes in the supernatant samples, the SPE
313 extracted samples were separated into two parts: flowthrough (part I) and SPE-extracted
314 (part II) samples. Substances with ionic or hydrophilic groups should flow through the
315 column (i.e., in part I), while Part II should contain hydrophobic compounds. The
316 concentration of Mo in part II was higher than that in part I, suggesting that Mo was mainly
317 chelated with hydrophobic substances in the supernatant. However, for the 160 mg/L
318 mineral group with the highest Mo concentration, a significant fraction was in ionic or
319 hydrophilic form (Fig. 3b).

320 CAS assay was run to qualitatively explore the presence of siderophores in flow-through
321 and SPE-extracted fractions. Siderophores were not present in the flow-through fraction but

322 were detected in the SPE-extracted fraction, as indicated by the blue-orange color in all
323 biotic experimental groups (Fig. S4). These results indicated the presence of siderophores in
324 the negative and positive controls, and mineral group that were capable of binding both Fe
325 and Mo.

326 To identify and quantify these siderophores in the SPE-extracted supernatant samples, a
327 combination of Orbitrap LC-MS, HPLC, and LC-ICP-MS was used. Orbitrap LC-MS analysis
328 revealed two siderophores with the m/z values of 789.40 and 831.41, which were identified
329 as rhodopetrobactins A and B, respectively (Fig. S5) and have been shown to be capable of
330 binding both Fe and Mo (Baars et al. 2018). With DHBA as a standard, HPLC analysis
331 quantified the concentrations of these two siderophores. In the positive control, both
332 siderophores were at a low level (Fig.3c). In their absence (i.e., negative control), the
333 concentrations of rhodopetrobactin A and B significantly increased, reaching 32.2 μM and
334 8.6 μM, respectively (Fig. 3c). When 160 mg/L molybdenite was used as the sole Mo source,
335 the concentrations of rhodopetrobactin A and B were close to those in the negative control,
336 reaching 31.0 μM and 7.9 μM respectively. In the lower mineral concentration group, the
337 siderophore concentrations were over 70% lower.

338 Supporting these findings, LC-ICP-MS results showed a peak around 584 s in the 160
339 mg/L molybdenite group (Fig. S6a), slightly shifted relative to the Mo-protochelin standard at
340 630 s, suggesting the presence of Mo-chelating siderophore or metabolite (Sheng et al.
341 2023). Using protochelin as a standard, LC-ICP-MS estimated the concentration of Mo-
342 chelating metabolite to be 0.2 μM in the 160 mg/L mineral group (Fig. 3d). This value was
343 close to the Mo concentration in the SPE-extracted hydrophobic fraction (~0.2 μM) (Fig. 3b),
344 demonstrating a consistency between the two independent methods. No Mo-chelating
345 complex was observed in other groups (Fig. 3d), likely due to limited Mo release (Fig. 3b) or
346 siderophore production (Fig. 3c). These results together suggested that when anoxygenic
347 phototroph experienced scarcity of aqueous Mo, they secreted siderophores/metallophores
348 to facilitate Mo uptake from alternative sources such as mineral.

349

350 *3.4 Change in mineral surface chemistry after cell incubation*

351 No secondary mineral was detected after interaction of molybdenite with cells,
352 indicating that its mineral structure remained unchanged (Fig. S7). SEM images revealed
353 significant cell adherence to the surface of molybdenite (Fig. 4a). Bacterial secretions tended
354 to form network-like structures at the edge of the molybdenite (Fig. 4a). Elemental maps
355 showed that while there were no significant changes in Mo and S after interaction of
356 molybdenite with cells (Fig. 4b), Fe, C, and P were enriched (Fig. S8), likely due to attachment
357 of dissolved Fe, cells and their exudates to molybdenite surface.

358 To explore deeper into any chemical changes of molybdenite surface as a result of cell
359 interaction, surface-sensitive XPS and TOF-SIMS techniques were employed. The peaks of
360 Mo3d and S2s in XPS profiles of pure molybdenite (Fig. S9) were consistent with a previous
361 study (Amin et al. 2018). While no significant new peaks emerged after microbial incubation,
362 intensities of Mo and S peaks significantly decreased (Fig. S9b-1), suggesting that the
363 molybdenite surface was covered by cells or exudates (Sheng et al. 2023), thus diluting the
364 Mo and S signals. This was further supported by increases of the relative peak intensities of
365 C=O and C-O-C (Fig. S9b-2), suggesting adsorption of organic compounds on the molybdenite
366 surface.

367 ToF-SIMS results offered more detailed insights (Figs. 5, S10-S11). Consistent with the XPS
368 results, the intensities of Mo and S maps notably decreased after interaction with cells,
369 accompanied by a concomitant increase of the C intensity (Fig. 5). Due to the high molecular
370 weight (789.40 / 831.41), detection of rhodopetrobactins by TOF-SIMS was challenging
371 (Körsgen et al. 2016). Nonetheless, rhodopetrobactin fragments (e.g., $C_7H_6O_3^-$, $C_{11}N_2H_{16}O_3^+$)
372 were identified on molybdenite surface after cell incubation (Figs. 5 and S10). Moreover,
373 peak intensities of other organic compounds (e.g., $C_3H_5^+$, $C_4H_7^+$, $C_3H_8N^+$) significantly
374 increased on microbially reacted molybdenite surface relative to the pure molybdenite (Fig.
375 S11). These results underpinned the importance of microbial secretion in acquiring metals
376 from minerals by direct contact.

377

378 *3.5 Protein expression in response to molybdenite as the sole Mo source*

379 To further explore the effects of different Mo sources on nitrogen fixation at the
380 molecular level, proteomic analysis was performed on the treatments including negative
381 control, positive control, and molybdenite group (160 mg/L). (Fig. 6). Gene clusters for
382 rhodopetrobactins (RPA2386-2390), ABC transporter (RPA2382 and 2385), Mo-nitrogenase
383 (NifDKH), and Mo transport system (ModA RPA4717, RPA4719) were the major focus (Fig. 6a
384 and 6b).

385 Compared to the negative control, addition of Mo in both dissolved and mineral forms
386 significantly increased the expression of Mo-nitrogenase (NifDKH) (Fig. 6c), consistent with
387 the observed increase in nitrogen fixation rates (Figs. 1 and 2). Relative to the negative
388 control and molybdenite group, proteins involved in rhodopetrobactin biosynthesis
389 (RPA_2386) and an ABC transporter (RPA_2382, RPA_2385) were down regulated in the
390 positive control (Fig. 6c), consistent with reduced production of siderophores when aqueous
391 Mo and Fe were replete (Fig. 3c). Furthermore, Mo transport protein (ModA) was down
392 regulated when Mo was present in either dissolved or molybdenite forms. Interestingly, TonB
393 siderophore receptor systems were significantly down regulated in the positive control, while
394 there was no difference between the molybdenite and negative groups. Thus, there was no

need for transporting Mo-siderophore complexes into cells in the positive control, but such mechanism may be important in the negative and molybdenite experiments. In addition, there was no significant difference in these protein expression levels between the dissolved and mineral forms of Mo, although the positive group showed overall higher expressions. These findings suggested that the mineral form of Mo was as bioavailable as soluble Mo in regulating nitrogen fixation.

4. Discussion

4.1 Impact of molybdenum on nitrogen fixation

Bioavailable nitrogen, such as ammonium, is crucial for biosynthesis of proteins and nucleic acids in all life forms (Canfield et al. 2010). Over geological timescales, nitrogen fixation has been critical in supporting the Earth's expanding biosphere because this is the only process that converts inert N_2 to bioavailable ammonium. Abiotic nitrogen fixation, resulting from processes like lightning and volcanic eruptions, was estimated to yield around 2×10^8– 2×10^{10} mol N per year (Canfield et al. 2010). In contrast, today, the marine biosphere fixes approximately 10^{13} mol N per year (Ward 2012). Before the evolution of oxygenic photosynthesis, productivity on early Earth may have been smaller than today (Canfield et al. 2006). However, the presumed constancy of organic carbon burial since at least 3.5 Gyr suggests a high nitrogen demand, comparable to modern levels and far exceeding the amount of abiotically fixed nitrogen (Krissansen-Totton et al. 2015). Therefore, biological nitrogen fixation was perhaps the primary source of bioavailable nitrogen for both present-day and early biosphere (Canfield et al. 2010).

In the modern ocean, phosphorus and iron are considered the primary limiting factors for nitrogen fixation, but not Mo, due to its abundance (~107 nM) in seawater (Mills et al. 2004). However, Mo is limited in terrestrial environments due to its low concentration in the continental crust, natural fresh water, and high leaching rate (Barron et al. 2008; Smedley and Kinniburgh 2017). Evidence indicates that Mo availability restricts nitrogen fixation in modern terrestrial ecosystems, such as tropical and temperate soils (Barron et al. 2008). Similarly, in freshwater lakes such as Castle Lake in California (2-4 nM) and Esthwaite Lake in England (0.1-2.6 nM), Mo scarcity (below 20 nM) limits primary productivity (Glass et al. 2012).

By comparing different diazotrophs across geological time, regardless of whether they are early evolved anaerobic diazotrophs such as methanogens (e.g., *Methanocaldococcus*, *Methanosarcina*) and anoxygenic photosynthetic bacteria (e.g., *Rhodopseudomonas palustris*), or later evolved aerobic diazotrophs such as cyanobacteria (*Anabaena variabilis*) and aerobic diazotroph (e.g., *Azotobacter vinelandii*), their diazotrophic growth was largely inhibited when dissolved Mo is below 10 nM (Table S2) (Bellenger et al. 2008; Nishizawa et al.

2014; Zerkle et al. 2006). However, ancient diazotrophs such as methanogens and anaerobic photosynthetic bacteria have lower nitrogen fixation rates than cyanobacteria and modern diazotrophs. In order to achieve a comparable rate of nitrogen fixation, these ancient diazotrophs have to acquire more Mo, because our finding (Fig. 1), along with others (Bellenger et al. 2011; Glass et al. 2010; Nishizawa et al. 2014), demonstrated that higher Mo level can increase the rate of nitrogen fixation.

Both isotopic (Stueken et al. 2015) and phylogenetic evidence (Parsons et al. 2021) suggest that ancient nitrogen fixation (3.2-2.9 Ga) was performed by Mo-nitrogenase, despite low levels of soluble Mo in the ocean. Although hydrothermal vents and anoxic abiotic weathering in early marine environments were important in providing localized Mo, most of the released Mo in these environments likely remained in solid form (~90%) (Evans et al. 2023), keeping aqueous Mo concentrations relatively low on a global scale. Therefore, we argue that ancient diazotrophs may have had the ability to acquire Mo from solid rocks and minerals as an additional source to meet their high demand for Mo (Sheng et al. 2023; Srivastava et al. 2023).

4.2 Mechanisms of microbial uptake of molybdenum as a cofactor for nitrogen fixation

By using genetically modified mutant strain with Mo-nitrogenase only, we excluded the possibilities of Fe-only nitrogenase activation. Our findings suggested that in Mo-depleted environments, such as early Earth and modern terrestrial ecosystems, Mo-bearing minerals may have provided an additional Mo flux to promote biological nitrogen fixation. Diazotrophs develop specific strategies to acquire Mo from minerals.

Microbes can extract nutrients from minerals through direct contact, acidification, redox reactions, and/or secretion of chelates (Dong et al. 2022; Uroz et al. 2009). In the current study, acidification and redox reaction were unlikely, as pH did not decline and no changes in Mo or S speciation were observed (Fig. S9). Therefore, direct contact and secretion of chelates should be the primary mechanisms at play.

Direct contact between minerals and microorganisms is essential for microbial uptake of nutrients from minerals (Ahmed and Holmström 2015). Our previous studies showed that growth of aerobic and anaerobic diazotrophs (*Azotobacter vinelandii* and *Clostridium kluyveri*) was inhibited when cells and molybdenite were physically separated by a dialysis bag (Sheng et al. 2023; Srivastava et al. 2023), underscoring the importance of direct contact for metal uptakes. Comparably, *R. palustris* demonstrated a high affinity for molybdenite surface (Fig. 4), despite both molybdenite and *R. palustris* surfaces are negatively charged. Such a tight physical contact would be difficult even with electrostatic attraction between mineral surfaces and cells (Sheng et al. 2021), unless the mineral could provide a growth benefit. Therefore, *R. palustris* may have overcome electrostatic repulsion to tightly adhere to

469 molybdenite surface, because of the strong need for Mo. Indeed, *R. palustris* has a greater
470 preference for anionic metals over cationic ones (Pokrovsky et al. 2014), underpinning its
471 strong nutritional needs regardless of the surface charge. This preference also suggested its
472 preponderance on early Earth, wherein the majority of trace metals exist as anionic sulfuric
473 species (Phillips and Xu 2021).

474 Secretion of chelates is another possible mechanism for Mo uptake. While *R. palustris*
475 has been shown to secrete siderophores when iron is limited (Baars et al. 2018), our results
476 showed that siderophores were secreted when molybdenite was the sole Mo source, even
477 when iron was abundant. This indicated a molybdenite-dependent siderophore secretion
478 system, as evidenced by increased rhodopetrobactin levels in the presence of high mineral
479 concentration (Fig. 3c). One possible explanation is that as the concentration of molybdenite
480 increased, more molybdenite surface became available for *R. palustris* cells, to acquire Mo
481 through secretion of rhodopetrobactin. This result, when combined with evidence of
482 microbial attachment, suggested that microbial attachment to mineral surface increased
483 siderophore secretion (Ahmed and Holmström 2015) and mineral dissolution. Aerobic
484 diazotrophs like *Azotobacter vinelandii* use similar strategies to acquire limiting metals,
485 controlling metal speciation and maintaining optimal cell-associated metal concentrations
486 for nitrogen fixation (McRose et al. 2017).

487 Secretion of siderophores results in the formation of Mo-siderophore complexes, but
488 they are too large to pass directly through porin channels on cell surface, and as a result,
489 specific transportation pathways are required to deliver the complexes into the cytoplasm
490 (Wiener and Horanyi 2011). The genome of *R. plaustris* encodes outer membrane
491 siderophore receptor systems such as transperiplasmic TonB (Larimer et al. 2004), which may
492 be required for transporting siderophores and metal-siderophore complexes into cells (Mirus
493 et al. 2009). Indeed, a significantly higher expression of TonB siderophore receptor proteins
494 was observed in the negative and mineral groups relative to the positive control (Fig. 6c),
495 consistent with the high siderophore production in the negative control (Fig. 3c) and Mo-
496 siderophore complex in the presence of molybdenite (Fig. 3d). This is consistent with the
497 finding that Fe-siderophore/Cu-methanobactin complexes could be transported into the cell
498 as a unit (Balasubramanian et al. 2011; Stintzi et al. 2000).

499 Alternatively, Mo may be assimilated into the cells by the periplasmic binding protein
500 ModA (Duhme-Klair 2009) when Mo is dissociated from the Mo-siderophore complexes. In *R.*
501 *palustris*, Mo ion uptake is regulated by transcription factor (ModE), which represses ModA
502 expression at micromolar Mo concentrations or higher, indicating that the ModA transporter
503 is synthesized only under low Mo conditions (Demtroder et al. 2019), such as the Mo-
504 depleted negative control in this study. Indeed, whether Mo was supplied in dissolved or
505 mineral forms, the expression of ModA for Mo ion transport was suppressed (Fig. 6),
506 because of adequate supplies of aqueous Mo (>0.1 μM) (Fig. 2).

4.3 Implication of bioavailability of Mo-bearing minerals on early Earth

The conditions that gave rise to nitrogen fixation and sustained its evolutionary development remain a subject of debate. It has been suggested that the first nitrogenase in the early biosphere was “proto-nitrogenase”, ancestral to the current forms and not so specific to nitrogen fixation (Mus et al. 2019). With the increase of ammonia demand by the expanding biosphere, more efficient Mo-nitrogenase evolved, which provides a survival advantage for life under the conditions of nitrogen limitation. At the same time, a high affinity Mo uptake system may have evolved to support the activity of Mo-nitrogenase (Lee et al. 2024). Therefore, despite the scarcity of dissolved Mo prior to the GOE, the kinetic advantage of Mo-nitrogenase may have favored its use as a cofactor over more abundant but less efficient alternatives like later evolved V and Fe nitrogenases. Our results provide a plausible explanation that mineral-associated Mo was bioavailable to early diazotrophs to sustain nitrogen demand and biosphere expansion.

Anoxygenic photosynthetic bacteria may have dominated the ocean’s primary productivity throughout much of the Archean (Planavsky et al. 2021). Prior to the emergence of oxygen-producing photosynthesis, anaerobic phototrophs likely dominated the entire photosynthetic niche (Ozaki et al. 2019). These bacteria may have played a crucial role in the early carbon and nitrogen cycles, populating in ecological niches located deep within the eutrophic zone (Johnston et al. 2009). They can thrive in low light conditions and utilize upwelling nutrients such as hydrogen, hydrogen sulfide, and ferrous iron (Kappler et al. 2005). Given the lower atmospheric thickness on early Earth (Catling and Zahnle 2020), the eutrophic zone was likely deeper than it is today. Our results highlight that in these early photic environments rich in Mo-bearing minerals and anoxygenic phototrophs, such as land, ocean basin boundaries, marginal basins (shallow seas) (Siebert et al. 2006), and continental margins (continental shelves) (McManus et al. 2006), Mo-bearing minerals would have provided an additional flux for primary productivity.

There is no direct evidence about the evolution of molybdophores (siderophores that bind molybdenum) on early Earth. However, we can infer some relevant information (Lee et al. 2024). The origin of siderophores may predate the GOE, as siderophore-synthesizing machineries are present across cyanobacteria (Wade et al. 2021), which originated at ~ 3.0 Ga (Planavsky et al. 2014). Early life in the surface photic zone likely experienced fluctuating iron solubilities, including those environments where iron was concentrated in solid phases (Canfield et al. 2006). Therefore, banded iron formations (BIFs), resulting from the oxidation of ferrous iron by anoxygenic phototrophic precipitation or abiogenic photooxidation, are not limited to the GOE interval but occurred intermittently during the Archaean (Kappler et al. 2005; Ozaki et al. 2019). This suggests that life in ancient anoxic environments may have developed an ability to acquire Fe(III) in solid form (Lee et al. 2024). While cyanobacteria

mostly secrete hydroxamate siderophore, Mo would have been only complexed with catechol siderophores, such as the rhodopetrobactins produced by *R. palustris*. Therefore, our results demonstrate that the molybdophores may have evolved early in response to Mo scarcity. Anaerobes capable of secreting molybdophores may have had a competitive advantage in utilizing solid-bound Mo, enhancing their nitrogen fixation capacities.

5. Conclusion

To better understand whether Mo-bearing mineral could as a potential Mo source to support Mo-nitrogenase, we conducted an experiment with a model Precambrian anoxygenic phototroph *R. palustris*, under anaerobic diazotrophic conditions using molybdenite as the sole Mo source. Our findings demonstrate that molybdenite can indeed support nitrogen fixation by *R. palustris*, with the rate of nitrogen fixation increasing in correlation with the concentration of molybdenite. Notably, under conditions of molybdenum scarcity, *R. palustris* is capable of secreting metallophores to extract the required Mo from minerals. This discovery could potentially resolve the paradox of the widespread presence of Mo-nitrogenase enzymes despite scarcity of aqueous Mo on early Earth.

Acknowledgments

This work was supported by grants from the National Science Foundation of China (42192500 and 42192503) and Fundamental Research Funds for the Central Universities (2652023001). The authors thank the Analysis Center, Department of Chemistry, Tsinghua University, and Dr. Liuqin Huang for their help with the TOF-SIMS analysis. We are grateful to Editor, Dr. Eva Stüeken and one anonymous reviewer whose comments improved the quality of the manuscript.

References

Ahmed E, Holmström SJM (2015) Microbe–mineral interactions: The impact of surface attachment on mineral weathering and element selectivity by microorganisms. Chemical Geology 403:13-23 doi:10.1016/j.chemgeo.2015.03.009

Amin R, Hossain MA, Zakaria Y (2018) Interfacial Kinetics and Ionic Diffusivity of the Electrodeposited MoS(2) Film. ACS Appl Mater Interfaces 10(16):13509-13518 doi:10.1021/acsami.8b01104

Anbar AD (2008) Elements and evolution. Science 322(5907):1481-1483 doi:10.1126/science.1163100

Baars O, Morel FMM, Zhang X (2018) The purple non-sulfur bacterium Rhodopseudomonas palustris produces novel petrobactin-related siderophores under aerobic and anaerobic conditions. Environ Microbiol 20(5):1667-1676 doi:10.1111/1462-2920.14078

Balasubramanian R, Kenney GE, Rosenzweig AC (2011) Dual Pathways for Copper Uptake by Methanotrophic Bacteria. Journal of Biological Chemistry 286(43):37313-37319 doi:10.1074/jbc.M111.284984

Barron AR, Wurzburger N, Bellenger JP, Wright SJ, Kraepiel AML, Hedin LO (2008) Molybdenum limitation of asymbiotic nitrogen fixation in tropical forest soils. Nature Geoscience 2(1):42-45 doi:10.1038/ngeo366

Bellenger JP, Wichard T, Kustka AB, Kraepiel AML (2008) Uptake of molybdenum and vanadium by a nitrogen-fixing soil bacterium using siderophores. Nature Geoscience 1(4):243-246 doi:10.1038/ngeo161

Bellenger JP, Wichard T, Xu Y, Kraepiel AM (2011) Essential metals for nitrogen fixation in a free-living N(2)-fixing bacterium: chelation, homeostasis and high use efficiency. Environ Microbiol 13(6):1395-411 doi:10.1111/j.1462-2920.2011.02440.x

Boyd ES, Anbar AD, Miller S, Hamilton TL, Lavin M, Peters JW (2011) A late methanogen origin for molybdenum‐dependent nitrogenase. Geobiology 9(3):221-232 doi:10.1111/j.1472-4669.2011.00278.x

Canfield DE, Glazer AN, Falkowski PG (2010) The evolution and future of Earth's nitrogen cycle. science 330(6001):192-196 doi:10.1126/science.1186120

Canfield DE, Rosing MT, Bjerrum C (2006) Early anaerobic metabolisms. Philosophical Transactions of the Royal Society B: Biological Sciences 361(1474):1819-1836 doi:10.1098/rstb.2006.1906

Cardona T (2019) Thinking twice about the evolution of photosynthesis. Open Biology 9(3) doi:10.1098/rsob.180246

Catling DC, Zahnle KJ (2020) The archean atmosphere. Science advances 6(9):eaax1420 doi: 10.1126/sciadv.aax1420

Cox Jr, Neuhauser N, Michalski A, Scheltema RA, Olsen JV, Mann M (2011) Andromeda: A Peptide Search Engine Integrated into the MaxQuant Environment. Journal of Proteome Research 10(4):1794-1805 doi:10.1021/pr101065j

David L. Huston, Carl W. Brauhart, Susan L. Drieberg, Garry J. Davidson, David I. Groves; Metal leaching and inorganic sulfate reduction in volcanic-hosted massive sulfide mineral systems: Evidence from the paleo-Archean Panorama district, Western Australia. Geology 2001;; 29 (8): 687–690. doi: 10.1130/0091-7613(2001)029<0687:MLAISR>2.0.CO;2

Demtroder L, Narberhaus F, Masepohl B (2019) Coordinated regulation of nitrogen fixation and molybdate transport by molybdenum. Mol Microbiol 111(1):17-30 doi:10.1111/mmi.14152

Dong H, Huang L, Zhao L, Zeng Q, Liu X, Sheng Y, Shi L, Wu G, Jiang H, Li F, Zhang L, Guo D, Li G, Hou W, Chen H (2022) A critical review of mineral-microbe interaction and co-evolution: mechanisms and applications. Natl Sci Rev 9(10):nwac128 doi:10.1093/nsr/nwac128

Doydora SA, Baars O, Harrington JM, Duckworth OW (2022) Salicylate coordination in metal-protochelin complexes. Biometals 35(1):87-98 doi:10.1007/s10534-021-00352-7

Duhme-Klair AK (2009) From Siderophores and Self-Assembly to Luminescent Sensors: The Binding of Molybdenum by Catecholamides. European Journal of Inorganic Chemistry 2009(25):3689-3701 doi:10.1002/ejic.200900416

Evans GN, Seyfried WE, Tan C (2023) Nutrient transition metals in a time series of hydrothermal vent fluids from Main Endeavour Field, Juan de Fuca Ridge, Pacific Ocean. Earth and Planetary Science Letters 602 doi:10.1016/j.epsl.2022.117943

Garcia AK, McShea H, Kolaczkowski B, Kacar B (2020) Reconstructing the evolutionary history of nitrogenases: Evidence for ancestral molybdenum-cofactor utilization. Geobiology 18(3):394-411 doi:10.1111/gbi.12381

Glass JB, Axler RP, Chandra S, Goldman CR (2012) Molybdenum limitation of microbial nitrogen assimilation in aquatic ecosystems and pure cultures. Frontiers in Microbiology 3 doi:10.3389/fmicb.2012.00331

Glass JB, Wolfe-Simon F, Elser JJ, Anbar AD (2010) Molybdenum—nitrogen co-limitation in freshwater and coastal heterocystous cyanobacteria. Limnology and Oceanography 55(2):667-676 doi:10.4319/lo.2010.55.2.0667

Greber ND, Mäder U, Nägler TF (2015) Experimental dissolution of molybdenum-sulphides at low oxygen concentrations: A first-order approximation of late Archean atmospheric conditions. Earth and Space Science 2(5):173-180 doi:10.1002/2014ea000059

Hao J, Sverjensky DA, Hazen RM (2019) Redox states of Archean surficial environments: The importance of H2,g instead of O2,g for weathering reactions. Chemical Geology 521:49-58 doi:10.1016/j.chemgeo.2019.05.022

Hazen RM, Liu X-M, Downs RT, Golden J, Pires AJ, Grew ES, Hystad G, Estrada C, Sverjensky DA (2014) Mineral evolution: episodic metallogenesis, the supercontinent cycle, and the coevolving geosphere and biosphere. doi:10.5382/SP.18.01

Helz GR, Bura-Nakić E, Mikac N, Ciglenečki I (2011) New model for molybdenum behavior in euxinic waters. Chemical Geology 284(3-4):323-332 doi:10.1016/j.chemgeo.2011.03.012

Johnson AC, Ostrander CM, Romaniello SJ, Reinhard CT, Greaney AT, Lyons TW, Anbar AD (2021) Reconciling evidence of oxidative weathering and atmospheric anoxia on Archean Earth. Science Advances 7(40):eabj0108 doi:10.1126/sciadv.abj0108

Johnston DT, Wolfe-Simon F, Pearson A, Knoll AH (2009) Anoxygenic photosynthesis modulated Proterozoic oxygen and sustained Earth's middle age. Proceedings of the National Academy of Sciences 106(40):16925-16929 doi:10.1073/pnas.0909248106

Kappler A, Pasquero C, Konhauser KO, Newman DK (2005) Deposition of banded iron formations by anoxygenic phototrophic Fe(II)-oxidizing bacteria. Geology 33(11) doi:10.1130/g21658.1

Knapp CW, Fowle DA, Kulczycki E, Roberts JA, Graham DW (2007) Methane monooxygenase gene expression mediated by methanobactin in the presence of mineral copper sources. Proceedings of the National Academy of Sciences 104(29):12040-12045 doi:10.1073/pnas.0702879104

Körsgen M, Tyler BJ, Pelster A, Lipinsky D, Dreisewerd K, Arlinghaus HF (2016) Changes in the molecular ion yield and fragmentation of peptides under various primary ions in ToF-SIMS and matrix-enhanced ToF-SIMS. Biointerphases 11(2) doi:10.1116/1.4940911

Kraemer SM, Duckworth OW, Harrington JM, Schenkeveld WDC (2014) Metallophores and Trace Metal Biogeochemistry. Aquatic Geochemistry 21(2-4):159-195 doi:10.1007/s10498-014-9246-7

Krissansen-Totton J, Buick R, Catling DC (2015) A statistical analysis of the carbon isotope record from the Archean to Phanerozoic and implications for the rise of oxygen. American Journal of Science 315(4):275-316 doi:10.2475/04.2015.01

Larimer FW, Chain P, Hauser L, Lamerdin J, Malfatti S, Do L, Land ML, Pelletier DA, Beatty JT, Lang AS, Tabita FR, Gibson JL, Hanson TE, Bobst C, Torres JL, Peres C, Harrison FH, Gibson J, Harwood CS (2004) Complete genome sequence of the metabolically versatile photosynthetic bacterium Rhodopseudomonas palustris. Nat Biotechnol 22(1):55-61 doi:10.1038/nbt923

Lee CC, Górecki K, Stang M, Ribbe MW, Hu Y (2024) Cofactor maturase NifEN: A prototype ancient nitrogenase? Science Advances 10(24):eado6169 doi:10.1126/sciadv.ado6169

Liermann LJ, Guynn RL, Anbar A, Brantley SL (2005) Production of a molybdophore during metal-targeted dissolution of silicates by soil bacteria. Chemical Geology 220(3-4):285-302 doi:10.1016/j.chemgeo.2005.04.013

Manck LE, Park J, Tully BJ, Poire AM, Bundy RM, Dupont CL, Barbeau KA (2022) Petrobactin, a siderophore produced by Alteromonas, mediates community iron acquisition in the global ocean. ISME J 16(2):358-369 doi:10.1038/s41396-021-01065-y

McManus J, Berelson WM, Severmann S, Poulson RL, Hammond DE, Klinkhammer GP, Holm C (2006) Molybdenum and uranium geochemistry in continental margin sediments: Paleoproxy potential. Geochimica et Cosmochimica Acta 70(18):4643-4662 doi:10.1016/j.gca.2006.06.1564

McRose DL, Baars O, Morel FMM, Kraepiel AML (2017) Siderophore production in Azotobacter vinelandii in response to Fe-, Mo- and V-limitation. Environ Microbiol 19(9):3595-3605 doi:10.1111/1462-2920.13857

Mills MM, Ridame C, Davey M, La Roche J, Geider RJ (2004) Iron and phosphorus co-limit nitrogen fixation in the eastern tropical North Atlantic. Nature 429(6989):292-294 doi:10.1038/nature02550

Mirus O, Strauss S, Nicolaisen K, von Haeseler A, Schleiff E (2009) TonB-dependent transporters and their occurrence in cyanobacteria. BMC Biology 7(1) doi:10.1186/1741-7007-7-68

Mohr W, Grosskopf T, Wallace DW, LaRoche J (2010) Methodological underestimation of oceanic nitrogen fixation rates. PLoS One 5(9):e12583 doi:10.1371/journal.pone.0012583

Mus F, Colman DR, Peters JW, Boyd ES (2019) Geobiological feedbacks, oxygen, and the evolution of nitrogenase. Free Radical Biology and Medicine 140:250-259 doi:10.1016/j.freeradbiomed.2019.01.050

Nishizawa M, Miyazaki J, Makabe A, Koba K, Takai K (2014) Physiological and isotopic characteristics of nitrogen fixation by hyperthermophilic methanogens: Key insights into nitrogen anabolism of the microbial communities in Archean hydrothermal systems. Geochimica et Cosmochimica Acta 138:117-135 doi:10.1016/j.gca.2014.04.021

Oda Y, Samanta SK, Rey FE, Wu L, Liu X, Yan T, Zhou J, Harwood CS (2005) Functional Genomic Analysis of Three Nitrogenase Isozymes in the Photosynthetic Bacterium Rhodopseudomonas palustris. Journal of Bacteriology 187(22):7784-7794 doi:10.1128/jb.187.22.7784-7794.2005

Ozaki K, Thompson KJ, Simister RL, Crowe SA, Reinhard CT (2019) Anoxygenic photosynthesis and the delayed oxygenation of Earth's atmosphere. Nature Communications 10(1) doi:10.1038/s41467-019-10872-z

Parsons C, Stueken EE, Rosen CJ, Mateos K, Anderson RE (2021) Radiation of nitrogen-metabolizing enzymes across the tree of life tracks environmental transitions in Earth history. Geobiology 19(1):18-34 doi:10.1111/gbi.12419

Perez-Miranda S, Cabirol N, George-Tellez R, Zamudio-Rivera LS, Fernandez FJ (2007) O-CAS, a fast and universal method for siderophore detection. J Microbiol Methods 70(1):127-31 doi:10.1016/j.mimet.2007.03.023

Philippi M, Kitzinger K, Berg JS, Tschitschko B, Kidane AT, Littmann S, Marchant HK, Storelli N, Winkel LHE, Schubert CJ, Mohr W, Kuypers MMM (2021) Purple sulfur bacteria fix N2 via molybdenum-nitrogenase in a low molybdenum Proterozoic ocean analogue. Nat Commun 12(1):4774 doi:10.1038/s41467-021-25000-z

Phillips R, Xu J (2021) A critical review of molybdenum sequestration mechanisms under euxinic conditions: Implications for the precision of molybdenum paleoredox proxies. Earth-Science Reviews 221 doi:10.1016/j.earscirev.2021.103799

Planavsky NJ, Asael D, Hofmann A, Reinhard CT, Lalonde SV, Knudsen A, Wang X, Ossa Ossa F, Pecoits E, Smith AJB, Beukes NJ, Bekker A, Johnson TM, Konhauser KO, Lyons TW, Rouxel OJ (2014) Evidence for oxygenic photosynthesis half a billion years before the Great Oxidation Event. Nature Geoscience 7(4):283-286 doi:10.1038/ngeo2122

Planavsky NJ, Crowe SA, Fakhraee M, Beaty B, Reinhard CT, Mills BJW, Holstege C, Konhauser KO (2021) Evolution of the structure and impact of Earth's biosphere. Nature Reviews Earth & Environment 2(2):123-139 doi:10.1038/s43017-020-00116-w

Pokrovsky OS, Martinez RE, Kompantzeva EI, Shirokova LS (2014) Surface complexation of the phototrophic anoxygenic non-sulfur bacterium Rhodopseudomonas palustris. Chemical Geology 383:51-62 doi:10.1016/j.chemgeo.2014.06.005

Rickard D (2012) Aqueous Metal–Sulfide Chemistry Sulfidic Sediments and Sedimentary Rocks. Developments in Sedimentology, pp 121-194

Rucker HR, Kacar B (2023) Enigmatic evolution of microbial nitrogen fixation: insights from Earth's past. Trends Microbiol doi:10.1016/j.tim.2023.03.011

Sánchez-Baracaldo P, Cardona T (2019) On the origin of oxygenic photosynthesis and Cyanobacteria. New Phytologist 225(4):1440-1446 doi:10.1111/nph.16249

Sheng Y, Baars O, Guo D, Whitham J, Srivastava S, Dong H (2023) Mineral-Bound Trace Metals as Cofactors for Anaerobic Biological Nitrogen Fixation. Environ Sci Technol doi:10.1021/acs.est.3c01371

Sheng Y, Dong H, Kukkadapu RK, Ni S, Zeng Q, Hu J, Coffin E, Zhao S, Sommer AJ, McCarrick RM, Lorigan GA (2021) Lignin-enhanced reduction of structural Fe(III) in nontronite: Dual roles of lignin as electron shuttle and donor. Geochimica et Cosmochimica Acta 307:1-21 doi:10.1016/j.gca.2021.05.037

Siebert C, McManus J, Bice A, Poulson R, Berelson WM (2006) Molybdenum isotope signatures in continental margin marine sediments. Earth and Planetary Science Letters 241(3-4):723-733 doi:10.1016/j.epsl.2005.11.010

Smedley PL, Kinniburgh DG (2017) Molybdenum in natural waters: A review of occurrence, distributions and controls. Applied Geochemistry 84:387-432 doi:10.1016/j.apgeochem.2017.05.008

Srivastava S, Dong H, Baars O, Sheng Y (2023) Bioavailability of mineral-associated trace metals as cofactors for nitrogen fixation by Azotobacter vinelandii. Geobiology doi:10.1111/gbi.12552

Stintzi A, Barnes C, Xu J, Raymond KN (2000) Microbial iron transport via a siderophore shuttle: a membrane ion transport paradigm. Proceedings of the National Academy of Sciences 97(20):10691-10696 doi:10.1073/pnas.200318797

Stueken EE, Buick R, Guy BM, Koehler MC (2015) Isotopic evidence for biological nitrogen fixation by molybdenum-nitrogenase from 3.2 Gyr. Nature 520(7549):666-9 doi:10.1038/nature14180

Stüeken EE, Kipp MA, Koehler MC, Buick R (2016) The evolution of Earth's biogeochemical nitrogen cycle. Earth-Science Reviews 160:220-239 doi:10.1016/j.earscirev.2016.07.007

Uroz S, Calvaruso C, Turpault M-P, Frey-Klett P (2009) Mineral weathering by bacteria: ecology, actors and mechanisms. Trends in Microbiology 17(8):378-387 doi:10.1016/j.tim.2009.05.004

Wade J, Byrne DJ, Ballentine CJ, Drakesmith H (2021) Temporal variation of planetary iron as a driver of evolution. Proceedings of the National Academy of Sciences 118(51) doi:10.1073/pnas.2109865118

Ward B (2012) The global nitrogen cycle. Fundamentals of geobiology:36-48 doi:10.1002/9781118280874.ch4

Wiener MC, Horanyi PS (2011) How hydrophobic molecules traverse the outer membranes of Gram-negative bacteria. Proceedings of the National Academy of Sciences 108(27):10929-10930 doi:10.1073/pnas.1106927108

Yang J, Junium CK, Grassineau NV, Nisbet EG, Izon G, Mettam C, Martin A, Zerkle AL (2019) Ammonium availability in the Late Archaean nitrogen cycle. Nature Geoscience 12(7):553-557 doi:10.1038/s41561-019-0371-1

Zerkle AL, House CH, Cox RP, Canfield DE (2006) Metal limitation of cyanobacterial N2 fixation and implications for the Precambrian nitrogen cycle. Geobiology 4(4):285-297 doi:10.1111/j.1472-4669.2006.00082.x

Figure Captions

Fig.1. Relationship between nitrogen fixation rate and aqueous Mo concentration. (a) Biomass-normalized ethylene production rate (a proxy for nitrogen fixation rate) under varying aqueous Mo concentrations. (b) Correlations between ethylene production rate and supplied or cell-associated Mo concentrations. (c) Time-course change of aqueous Mo concentration across different Mo concentration groups. (d) Cell-associated Mo concentration across different Mo concentration groups. Error bars represent one standard deviation from triplicate experiments.

Fig.2. Relationship between nitrogen fixation rate and solid-source Mo concentration. (a) Growth curve of *R. palustris* CGA009-Δ*anfA* measured by OD_{600nm} in the molybdenite experiments. (b) Biomass-normalized ethylene production rate (bar graph) and N_2 fixation rate (curve). (c) Time-course change of extracellular aqueous Mo concentrations (defined as the difference in aqueous Mo between later time points and time zero). (d) Biomass-normalized cell-associated Mo concentrations. Error bars represent one standard deviation from triplicate experiments. ND denotes no detection.

Fig.3. Characterization and quantification of metallophores. (a) Mo release when molybdenite was incubated with supernatant samples for 24 hours under anoxic conditions. Negative control supernatant and mineral group supernatant collected from the negative control (-Fe -Mo) and molybdenite experiment (160 mg/L), respectively. (b) Mo concentrations in flow-through and SPE-extracted fractions after solid phase extraction (SPE) of the experimental supernatant samples. SPE-extracted samples were separated into two parts: flowthrough and SPE-extracted samples. (c) Concentrations of rhodopetrobactin A and rhodopetrobactin B in the SPE-extracted samples as determined by HPLC. (d) Concentrations of Mo-chelating metabolites in the SPE-extracted samples as determined by LC-ICP-MS. ND represents no detection.

Fig.4. (a) SEM images showing attachment of *R. palustris* CGA009-Δ*anfA* to molybdenite surface in the molybdenite experiments (160 mg/L). (b) SEM images and elemental maps showing the Mo, S, Fe, P, C, N enrichments on molybdenite surfaces after interaction with *R.palustris* CGA009-Δ*anfA* cells.

Fig.5. ToF-SIMS maps showing the intenisty of Mo (a, b), S (c, d), C (e, f), $C_7H_6O_3^-$ (g, h) on molybdenite surface before and after interaction with *R.palustris* cells. $C_7H_6O_3^-$ represents

828 the fragments of rhodopetrobactins A and B. The color gradient from black to yellow
829 represents increased intensity.

830

831 Fig.6. (a) Operon structures of siderophore biosynthesis genes (production: RPA2386-
832 RPA2390, ABC transport: RPA2382 and RPA2385), Mo-nitrogenase genes(nifDKH), Mo-
833 transport genes (modA, RPA4719), and TonB siderophore receptor systems (RPA2378,
834 RPA2380) encoded in *R. plausrtis CGA009-Δ*anfA*. (b) Volcano plots revealing the significant
835 difference in protein expression levels (Log_2 fold change < -2 or >2, $p<0.05$) in the pairwise
836 comparison between positive control (+Fe +Mo) vs. negative control (-Fe -Mo), positive
837 control (+Fe +Mo) vs. molybdenite, molybdenite vs. negative control (-Fe -Mo). (c) Difference
838 in protein expression (log_2 fold change) between pairwise experimental groups. The color
839 gradient from blue to red represents down-regulated to up-regulated protein expressions.
840 The asterisk represents significant diffrerence ($p < 0.05$).

841

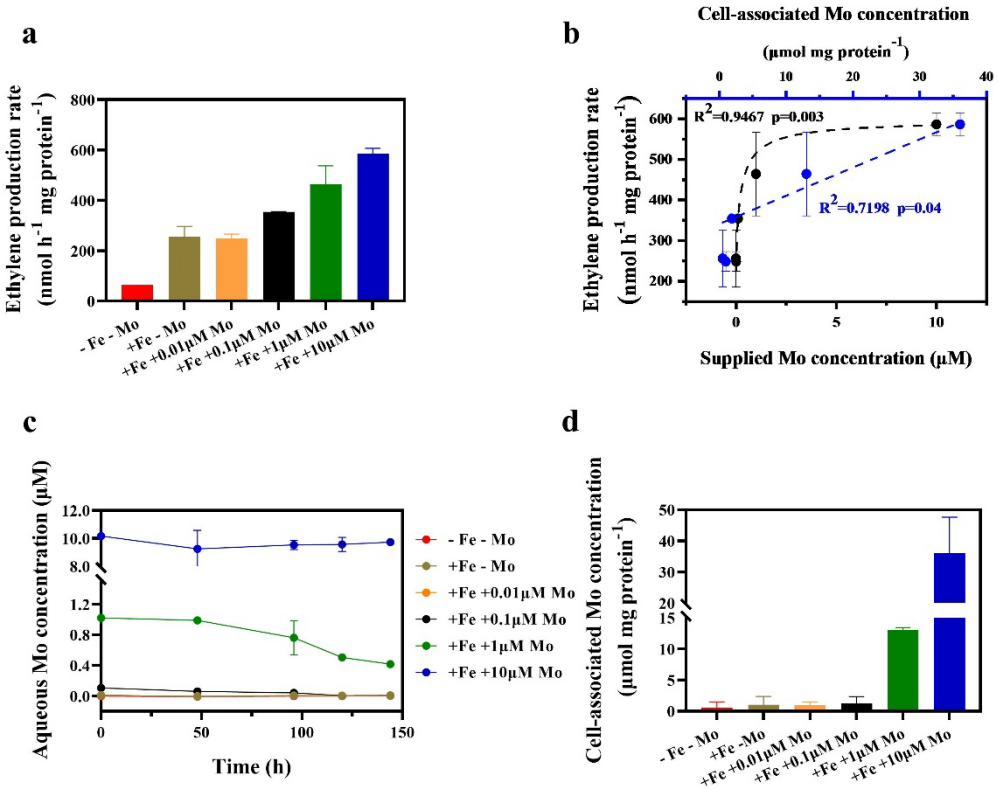
a
Ethylene production rate (nmol h-1 mg protein-1)
800
600
400
200
0
- Fe - Mo
+Fe - Mo
+Fe +0.01μM Mo
+Fe +0.1μM Mo
+Fe +1μM Mo
+Fe +10μM Mo
b
Cell-associated Mo concentration (μmol mg protein-1)
0
10
20
30
40
Ethylene production rate (nmol h-1 mg protein-1)
600
500
400
300
200
R2=0.9467 p=0.003
R2=0.7198 p=0.04
0
5
10
Supplied Mo concentration (μM)
c
Aqueous Mo concentration (μM)
12.0
10.0
8.0
1.2
0.8
0.4
0.0
0
50
100
150
Time (h)
- Fe - Mo
+Fe - Mo
+Fe +0.01μM Mo
+Fe +0.1μM Mo
+Fe +1μM Mo
+Fe +10μM Mo
d
Cell-associated Mo concentration (μmol mg protein-1)
50
40
30
20
15
10
5
0
- Fe - Mo
+Fe -Mo
+Fe +0.01μM Mo
+Fe +0.1μM Mo
+Fe +1μM Mo
+Fe +10μM Mo

Figure 1

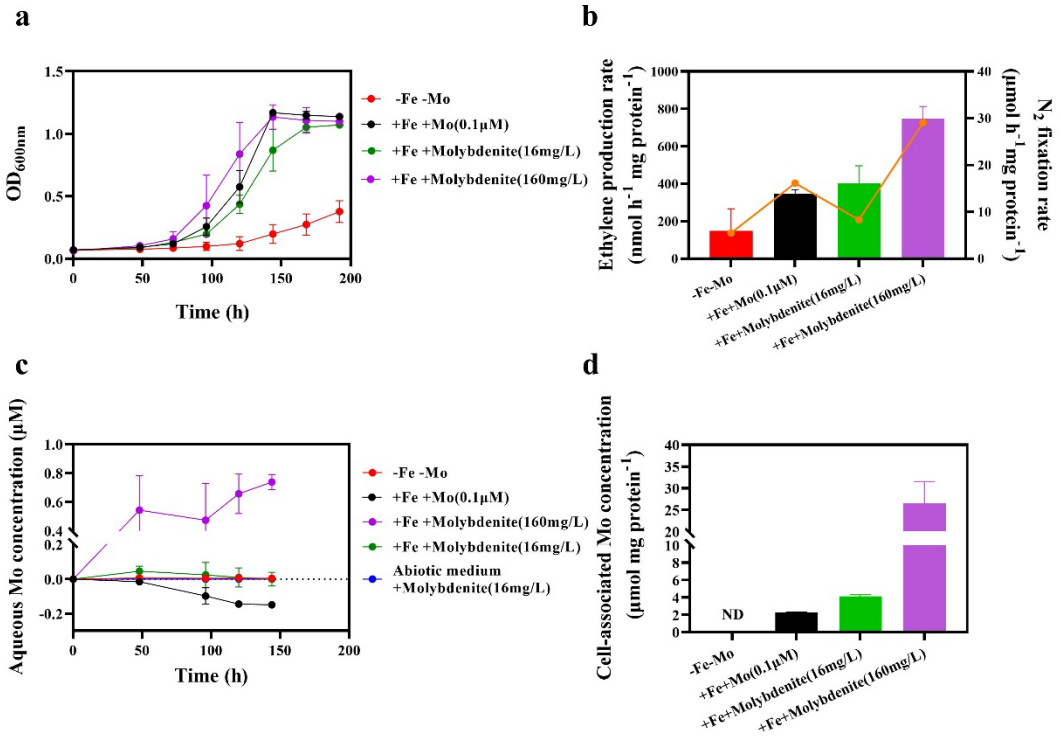
a
b
c
d
OD600nm
Time (h)
-Fe -Mo
+Fe +Mo(0.1μM)
+Fe +Molybdenite(16mg/L)
+Fe +Molybdenite(160mg/L)
Ethylene production rate (nmol h-1 mg protein-1)
N2 fixation rate (μmol h-1 mg protein-1)
Aqueous Mo concentration (μM)
Abiotic medium +Molybdenite(16mg/L)
Cell-associated Mo concentration (μmol mg protein-1)
ND

Figure 2

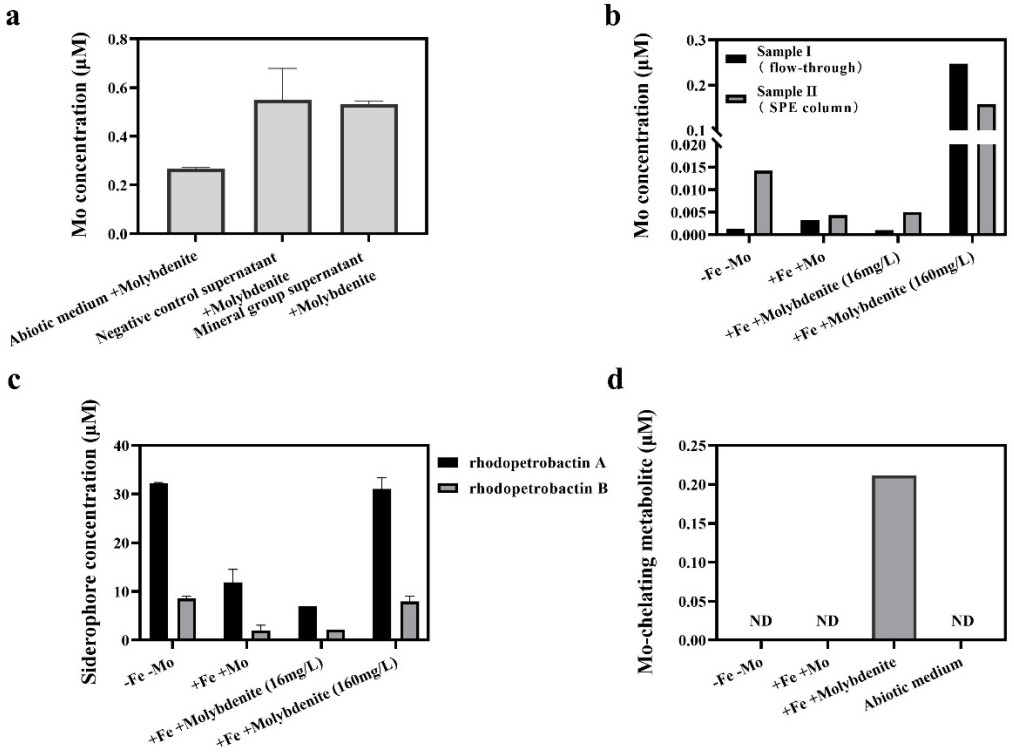
a
Mo concentration (μM)
0.8
0.6
0.4
0.2
0.0
Abiotic medium +Molybdenite
Negative control supernatant +Molybdenite
Mineral group supernatant +Molybdenite
b
Mo concentration (μM)
0.3
0.2
0.1
0.020
0.015
0.010
0.005
0.000
Sample I (flow-through)
Sample II (SPE column)
-Fe -Mo
+Fe +Mo
+Fe +Molybdenite (16mg/L)
+Fe +Molybdenite (160mg/L)
c
Siderophore concentration (μM)
40
30
20
10
0
rhodopetrobactin A
rhodopetrobactin B
-Fe -Mo
+Fe +Mo
+Fe +Molybdenite (16mg/L)
+Fe +Molybdenite (160mg/L)
d
Mo-chelating metabolite (μM)
0.25
0.20
0.15
0.10
0.05
0.00
ND
ND
ND
-Fe -Mo
+Fe +Mo
+Fe +Molybdenite
Abiotic medium

Figure 3